Available online at www.sciencedirect.com
SCIENCE DIRECT®
Journal of Nuclear Materials 326 (2004) 9–18
journal of nuclear materials
www.elsevier.com/locate/jnucmat

Morphological evolution of alteration layers formed during nuclear glass alteration: new evidence of a gel as a diffusive barrier

Diane Rebiscoul [a,*], Arie Van der Lee [b], Francois Rieutord [c], Frédéric Né [c], Olivier Spalla [d], Abdeslam El-Mansouri [b], Pierre Frugier [a], André Ayral [b], Stéphane Gin [a]

[a] *Commissariat à l'Energie Atomique (CEA), Centre de Recherche de la Vallée du Rhône, DEN/DIEC/SESC/ Laboratoire d'Etude du Comportement à Long Terme, BP 17171, 30207 Bagnols-sur-Cèze cedex, France*
[b] *Institut Européen de Membranes, UMR CNRS 5635, CC047, Université Montpellier II, Place Eugène Bataillon, 34095 Montpellier cedex 5, France*
[c] *Commissariat à l'Energie Atomique (CEA), DSM/DRFMC/SI3M/PCM, 17 rue des Martyrs, F-38054 Grenoble cedex, France*
[d] *Commissariat à l'Energie Atomique (CEA), DSM/DRECAM/SCM, Bât 125, F-91191 Gif-sur-Yvette, France*

Received 16 July 2003; accepted 30 October 2003

Abstract

This paper presents X-ray reflectometry and nitrogen adsorption results on alteration films formed at the surface of the French high level radioactive waste reference glass: SON68 glass (R7T7-type). For the first time, in situ (underwater) X-ray reflectometry has been used to investigate the alteration of this nuclear glass. A morphological evolution of alteration films is proposed and related to different steps of alteration kinetics. Initially a de-alkalinized glass layer is obtained, followed by the formation of a gel having an open porosity. Subsequently the gel densifies as the glass alteration rate decreases and finally the pore size increases upon formation of a dense and thin zone within the film. The latter dense zone within the gel could constitute a diffusive barrier. This hypothesis is also discussed for simplified glass gels.

1. Introduction

Studying glass alteration mechanisms is required to build predictive models for long-term behavior of high level waste (HLW) glass in disposal conditions. During HLW glass dissolution, an alteration film is observed. For the SON68 glass, a R7T7-type nuclear glass [1], this film consists of de-alkalinized glass, a gel [2] and crystalline phases, like phyllosilicates and rare earth phosphates [3,4]. For alteration between 50 and 100 °C, the gel is the most important component of the alteration film. It is an amorphous and hydrated material formed by recondensing crosslinking species (Si, Al, etc.). This gel tends to retain long-lived radioactive species contained in the glass and leads to a decrease of four orders of magnitude of the alteration rate compared with the initial dissolution rate [5–8]. Gel features depend on glass composition [9] and alteration conditions [10]. Predictive models [11] take into account the protective properties of the gel. In order to enhance the robustness of these models, the knowledge of gel protective properties and its evolution during alteration should be thoroughly studied.

A previous study showed the formation of a complex density gradient within the gel during alteration [12]. In

* Corresponding author. Tel.: +33-04 66 79 69 04; fax: +33-04 66 79 66 20.
E-mail address: diane.rebiscoul@cea.fr (D. Rebiscoul).

0022-3115/$ - see front matter © 2003 Elsevier B.V. All rights reserved.
doi:10.1016/j.jnucmat.2003.10.015

order to understand the gradient nature, X-ray reflectometry (XRR) and nitrogen adsorption analyses have been carried out on alteration films at different reaction times. Experimental results are presented and a possible morphological evolution of the alteration films of SON68 glass and simplified glasses (glasses 1 and 2) is proposed.

2. Materials and methods

2.1. Sample preparation

The main glass used is the SON68 glass [1], a R7T7-type nuclear glass, whose composition is detailed in Table 1. Two simplified glasses (glasses 1 and 2), with the same primary components and the same molar ratio as the SON68 glass [9] are also studied (Table 1). Glass 1 has an initial dissolution rate in pure water ($r_{0(90\,^{\circ}C,\,pH=9)} = 2.4\ g\,m^{-2}\,day^{-1}$) close to that of SON68 ($r_{0(90\,^{\circ}C,\,pH=9)} = 2.2\ g\,m^{-2}\,day^{-1}$). In static mode, this glass is approximately two or three times more altered than SON68 glass (thickness) and presents a continuous decrease of the alteration rate [9]. The dissolution rate of glass 2 is higher ($r_{0(90\,^{\circ}C,\,pH=9)} = 8.5\ g\,m^{-2}\,day^{-1}$) [9] and an abrupt stop of alteration can be observed as shown in Fig. 1. Alteration films of these two glasses do not contain crystalline phases on the gel surface.

Monoliths of these three glasses measuring $25\times25\times2.5\ mm^3$ were cut from a large glass bar and polished to grade 4000 with SiC paper. Monoliths were then ultrasonically cleaned, first in acetone, in ethanol and finally in deionized water. Powders were prepared by grinding and sieving monolith glass blocks. Size fractions obtained were 63–100 μm for SON68 glass, 5–20 μm for glass 1 and 40–63 μm for glass 2. These fractions were cleaned following the same procedure as for the monoliths. Specific surface areas measured by krypton adsorption were 0.064 ± 0.001, 0.337 ± 0.001 and $0.173\pm0.001\ m^2\,g^{-1}$, respectively. Furthermore, the glass-surface-area-to-solution-volume ratio (S/V) influences the alteration kinetics whereas the specific surface area differences for these fractions size have no such influence.

Table 1
Composition (wt%) of SON68 and simplified glasses 1 and 2 [9]

Oxide	Glass SON68	Glass 1	Glass 2
SiO_2	45.48	58.07	59.80
Al_2O_3	4.91	6.27	
B_2O_3	14.02	17.92	18.45
Na_2O	9.86	12.59	12.95
CaO	4.04	5.15	5.31
Li_2O	1.98		
ZnO	2.50		
ZrO_2	2.65		3.49
Fe_2O_3	2.91		
NiO	0.74		
Cr_2O_3	0.51		
P_2O_5	0.28		
Others	10.12		

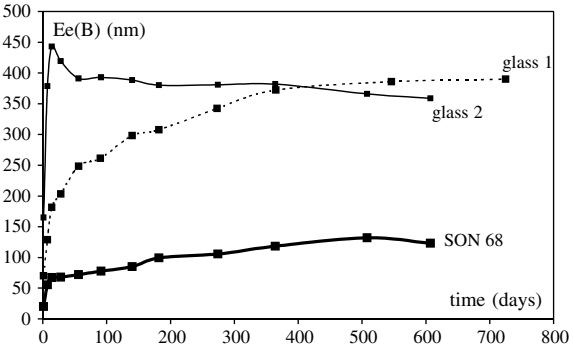

Fig. 1. Altered glass thickness Ee(B) evolution as a function of time for glasses 1, 2 and SON68 altered at 90 °C and $S/V = 8000\ m^{-1}$ [9].

The experiments were carried out in static mode and in a PTFE reactor at $S/V = 8000\ m^{-1}$. Before powders were added, ultrapure water solutions were heated during 2 h in an oven regulated at 90 ± 2 °C. Glass monoliths were altered within glass powder in order to ensure the same alteration rate for the monolith and for the powder by avoiding local concentration effects. All tests are detailed in Table 2. The reactors were put during alteration in an oven at 90 ± 1 °C. Monolith, powder and solution samples were taken from the reactor at the same time. Subsequently solution samples were ultrafiltered to 10.000 Da and diluted in an equivalent volume

Table 2
Summary report of different experiments performed at 90 °C, $S/V = 8000\ m^{-1}$ and characterization conditions for monoliths and powders related to each tests

Test	Time (day)	Analysis conditions	
		Monolith	Powder
SON68-0.4	0.4	w d	d
SON68-4	4	w d	d
SON68-7	7	w d	d
SON68-21	21	w d	d
SON68-62	62	w d	d
Glass 1	62	d	na
Glass 2	62	d	na

w: wet, d: dry, na: not analyzed.

of 1 N HNO_3. Acidified solutions were analyzed by plasma atomic emission spectroscopy in order to determine atomic concentrations. For in situ characterization, monoliths were collected and directly put in the analysis cell. After characterization, monoliths were rinsed with ultrapure water and dried in laboratory atmosphere. The same dried surfaces were then analyzed. Powders were rinsed with 8 ml of ultrapure water and dried in laboratory atmosphere.

2.2. Characterizations

Concentrations in solution were determined by plasma atomic emission spectroscopy for Si, B, Na, Li, Al, Ca. The precision is roughly 5% when the concentrations are above the detection limit (0.05 mg l^{-1}). After correcting the concentration values by the dilution factor that is due to dilution in the acid solution, the normalized mass losses NL_i (g m^{-2}) were calculated from the following relation (1):

$$NL_i = \frac{C_i}{x_i \cdot \frac{S}{V}}, \tag{1}$$

where C_i (mg l^{-1}) is the concentration of element i and x_i is the mass fraction of element i in the glass. NL_i (g m^{-2}) is used to estimate the altered glass thickness Ee(B) (μm) calculated from a mobile element (B, Na) (2):

$$\mathrm{Ee(B)} = \frac{NL_i}{\rho_V}, \tag{2}$$

ρ_V (g cm^{-3}) is the glass density.

The density of the altered glass ρ_{SA} (g cm^{-3}) (3) corresponds to a glass in which the oxides are dissolved in a volume corresponding to the thickness of the altered glass Ee(B):

$$\rho_{SA} = \frac{m_V - m_{oxy}}{m_V}\rho_V, \tag{3}$$

where m_V (g) is the glass mass and m_{oxy} (g) is the dissolved oxide mass in solution.

The mass of altered film per surface area unit m_{SA} (10^{-3} g m^{-2}) is defined by the following expression (4):

$$m_{SA} = \rho_{SA} \times \mathrm{Ee(B)} \times S_{spe}, \tag{4}$$

where S_{spe} (m^2 g^{-1}) is the specific surface area.

Nitrogen adsorption measurements on altered glass powder were carried out using a conventional volumetric apparatus Micromeritics ASAP 2010. Classical characteristics related to the porosity of the sample were obtained from isotherms such as pore volume, specific surface area determined by the BET method and the average pore size by the BJH model using the adsorption branch of the isotherm curve [13]. Data are first presented for a mass of altered glass powder in order to have the specific surface area and pore volume for the total mass of glass, and secondly, for a mass of altered glass using the mass m_{SA} as defined before (4).

Density ρ_R and thickness e_R of alteration film on monoliths were obtained from X-ray reflectivity measurements. Reflectivity values are related to the electron density of the layer and its substrate [14]. In situ measurements were done at the European Synchrotron Radiation Facility (ESRF) on the BM32 French beam line (CRG-IF). The energy of the incident beam was 20.05 keV. The detector system is a NaI scintillator coupled with a photomultiplier tube. Samples were placed in a special cell equipped with two Nalophan® windows.

XRR measurements on dried samples were obtained with a Brucker D5000 diffractometer equipped with a special reflectivity stage and a graphite monochromator in the reflected beam. Cu-$L_{3,2}$ ($\lambda = 0.15051$ and 0.15433 nm) radiation and standard θ–2θ scan were used for the data collections. The reflectivity stage is essentially a beam-knife that cuts the beam in the center of the goniometer and thus reduces the effective reflective area. This area depends on the incident angle of the X-ray beam and on the size of the central slit between the lower side of the beam-knife and the sample surface. The central slit size was typically 15 μm. Step sizes and step times were variable and chosen according to the intensity measured during fast prescans in small angular intervals. Reflectivity curves are generally presented as the logarithmic evolution of the intensity received by the detector as a function of the incident θ angle. Details concerning XRR application on alteration film are available in [12].

All XRR-related calculations were performed with the program IMD 4.1 [15]. This program was used to adjust the experimental reflectivity curves to models in terms of density, thickness and roughness of a few layers. Fig. 2 shows the location of layers and their parameters ($\sigma_{i/j}$: interfacial roughness, e_{Ri}: layer thickness, ρ_{Ri}: layer density). First, layers and substrate densities are adjusted to the small angles experimental data points. Secondly thickness and roughness were adjusted to the full experimental curve. In our experimental conditions, the results are given with a precision of ±0.1 g cm^{-3} for ρ_{Ri}, and ±1 nm for e_{Ri}. For some simulations, an abrupt interface was replaced by a graded interface. A graded interface consists of one or more layers whose optical constants vary gradually between the values for the pure materials on either side of the interface. A graded interface is described by several parameters as shown in Fig. 2: the thickness of the graded interface e_{GI}, the number of layers comprising the graded interface n_G, the distribution

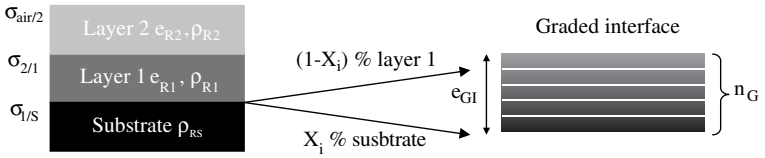

Fig. 2. Schematic representation and location of different layers simulated and description of the graded interface. e_{Ri}: layer i thickness; ρ_{Ri}: layer i density; e_{GI}: graded interface thickness; n_G: number of layers comprising the graded interface; X_i: distribution factor of the graded interface.

factor X_i which determines the location of the graded interface relatives to the original abrupt interface.

Ultramicrotome cross-section of altered glass 2 powder prepared according to the technique by Ehret et al. [16] were observed using a transmission electron microscope Philips CM 120 (TEM).

3. Results and discussion

Studies on SON68 glass alteration [16–18] showed that alteration kinetics in static conditions start by an ionic exchange between modifier cations from the glass and protons from the solution. This process is commonly called the interdiffusion process. The second step is the hydrolysis of the silicate network at an initial rate that depends on the matrix. The third step is characterized by a drop in the alteration rate by several orders of magnitude compared with the initial rate, then followed by a quasi-constant residual rate. The goal of this study is to relate the morphology of the alteration layer at the different alteration steps.

Fig. 3 and Table 3 show the thickness Ee(B) and the density ρ_{SA} of SON68 altered glass as a function of time. Density and porosity data for the altered glass are analyzed on monoliths and powders during these different alteration steps. Two kinds of analyses were done on SON68 altered glass. First, altered monoliths were analyzed by in situ and ex situ (i.e. on dried samples) XRR to obtain the density ρ_R and the thickness e_R of alteration film. Reflectivity curves obtained in situ and with dried monoliths are presented in Figs. 4 and 5, and simulation results of experimental curves are summarized in Table 4. Then, altered glass powders were analyzed by nitrogen adsorption in order to assess the open porosity. Data collected are summarized in Table 5. Pore size distributions of altered glass powders are presented in Fig. 6.

In the following analysis, several morphologies of SON68 glass alteration film are proposed and related to alteration steps (Fig. 7). The importance of the gel as a diffusive barrier is also discussed for alteration layers of the simplified glasses 1 and 2.

3.1. First step: interdiffusion step

As solution analysis shows (Table 3), after 8 h of reaction, the alteration rate drops by about one order of magnitude compared with the initial rate dissolution $(r_{0(90\,^{\circ}C,\,pH=9)}/20)$. The reflectivity curve of sample SON68-0.4 w in situ (Fig. 4) shows a low amplitude fringe. The best simulation corresponds to a graded

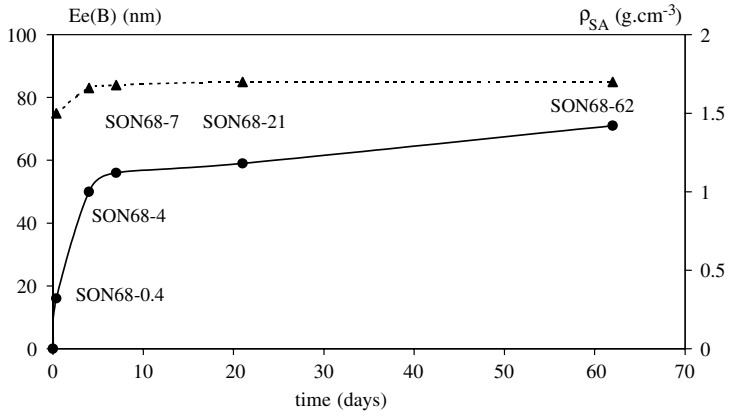

Fig. 3. Evolution of altered glass thickness Ee(B) (nm) – (●) and density determined by solution analysis ρ_{SA} (g cm^{-3}) – (▲). Different tests SON68-0.4 to SON68-62 are located on the figure.

Table 3
Alteration time for different experiments, thickness Ee(B) (nm), density ρ_{SA} ($g\,cm^{-3}$) of altered glass and rate drop $r_0/r(B)$ determined by solution analysis

Test	Time (day)	Ee(B) (nm)	ρ_{AS} ($g\,cm^{-3}$)	$r_0/r(B)$
SON68-0.4	0.4	16	1.50	20
SON68-4	4	50	1.66	80
SON68-7	7	56	1.68	360
SON68-21	21	59	1.70	4000
SON68-62	62	71	1.75	3000
Glass 1	62	147	1.70	1000
Glass 2	62	221	1.72	>10000

$r_{0(SON68)} = 2.2\ g\,m^{-2}\,j^{-1}$, $r_{0(glass\ 1)} = 2.4\ g\,m^{-2}\,j^{-1}$, $r_{0(glass\ 2)} = 8.5\ g\,m^{-2}\,j^{-1}$, $r(B) = \Delta NL(B)/\Delta t$.

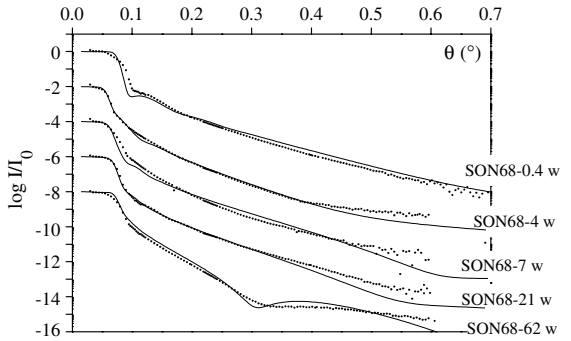

Fig. 4. Experimental and simulated reflectivity curves of altered SON68 glass in situ for samples SON68-0.4 w to SON68-62 w. The curves have been shifted vertically for the sake of clarity (X wave line $\lambda = 0.06184$ nm).

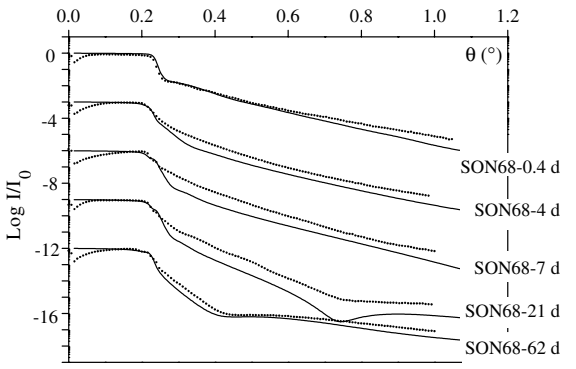

Fig. 5. Experimental and simulated reflectivity curves of altered SON68 glass after drying for samples SON68-0.4 d to SON68-62 d. The curves have been shifted vertically for the sake of clarity (X wave line $\lambda = 0.15433$ nm).

interface thickness similar to that of the layer, meaning a density gradient is in the whole alteration layer. The mean density varies from the glass density $\rho_S = 2.7\ g\,cm^{-3}$, to a density close to the one of de-alkalinized glass $\rho_R = 1.9\ g\,cm^{-3}$. Previous studies have already showed the formation of this interdiffusion layer [12]. The analyzed layer mainly consists of de-alkalinized glass and of a small amount of gel formed at close initial dissolution rate condition (step of initial dissolution rate is about 5 min). This gel contribution decreases the global density of the layer. The XRR results for dried sample SON68-0.4 d are similar as those for SON68-0.4 w. Drying has no measurable effect on this layer. The porosity analysis performed on the corresponding dried powder (Table 5) indicates a porosity with a mean pore diameter of 3.6 nm.

3.2. Second step: gel formation

After 4 days of alteration (test SON68-4), the drop in the alteration rate is moderate compared with the previous step ($r_{0(90\,°C,\,pH=9)}/80$) (Table 3). Simulation of the reflectivity curve for sample SON68-4 w shows that the thickness increases and the density of the alteration layer decreases. The density contrast for this sample is located between the layer and the de-alkalinized glass and not between the layer and the glass as in the previous test. The gel is the main component of the layer. For the dried sample SON68-4 d, a small layer contraction (5%) can be detected. Porosity analysis carried out on the corresponding dried powder shows a strong increase of both specific surface area and pore volume. The pore size distribution leads to a mean pore size of 5 nm. This value is of the same order of magnitude as the surface roughness found with reflectivity on the dried and in situ sample (SON68-4 w and SON68-4 d). At this reaction progress, the amount of altered glass still increases (Fig. 3), which means that fresh glass is still accessible to water. Consequently, the altered glass porosity which is measured can be applied to the total volume of the gel.

Thus, the alteration layer consists of a de-alkalinized glass layer and a gel with an open porosity with a mean pore diameter of 5 nm (Fig. 7).

Table 4
Reflectivity curves simulation results of in situ and dried altered monoliths

Sample	Layer 2			Layer 1			Substrate		Graded interface		
	$\sigma_{air/2}$ (nm)	e_{R2} (nm)	ρ_{R2} (g cm^{-3})	$\sigma_{2/1}$ (nm)	e_{R1} (nm)	ρ_{R1} (g cm^{-3})	$\sigma_{1/s}$ (nm)	ρ_S (g cm^{-3})	e_{GI} (nm)	n_G	X_i
SON68-0.4w	1.1 ± 0.2	18 ± 1	1.9 ± 0.1	–	–	–	2.0	2.7 ± 0.1	18	20	1% substrate
SON68-4w	5 ± 0.2	24 ± 1	1.5 ± 0.1	–	–	–	1.5	2.0 ± 0.1	1	10	50% substrate
SON68-7w	6 ± 0.5	35 ± 2	1.8 ± 0.1	–	–	–	1.0	2.2 ± 0.1	2	20	50% substrate
SON68-21w	7 ± 0.5	38 ± 2	1.8 ± 0.1				1.2	2.4 ± 0.1	2	20	50% substrate
SON68-62w	7 ± 0.5	36 ± 1	1.5 ± 0.1	1 ± 0.2	3 ± 0.5	1.9 ± 0.1	1.3	2.6 ± 0.1	1	20	50% substrate
SON68-0.4d	1.5 ± 0.2	18 ± 1	1.9 ± 0.1	–	–	–	2.0	2.6 ± 0.1	18	10	1% substrate
SON68-4d	6 ± 0.5	23 ± 2	1.7 ± 0.2	–	–	–	1.5	2.6 ± 0.1	1	10	1% substrate
SON68-7d	7 ± 0.5	33 ± 10	2.0 ± 0.2	–	–	–	1.5	2.6 ± 0.1	–	–	–
SON68-21d	8 ± 1	36 ± 1	2.2 ± 0.1	–	–	–	1.5	2.7 ± 0.1	5	10	50% substrate
SON68-62d	7 ± 0.5	27 ± 1	1.5 ± 0.1	2 ± 0.2	6 ± 0.5	2.0 ± 0.1	0.5	2.4 ± 0.1	25	10	60% layer 1
Glass 1	4 ± 0.5	250 ± 50	1.9 ± 0.1	0.8 ± 0.1	9 ± 0.5	2.2 ± 0.1	0.8 ± 0.1	2.6 ± 0.1	–	–	–
Glass 2	0.5 ± 0.1	19 ± 1	1.3 ± 0.1	3 ± 0.2	370 ± 30	0.8 ± 0.1	0.5 ± 0.1	2.0 ± 0.1	–	–	–

e_{Ri}: layer i thickness; ρ_{Ri}: layer i density; e_{GI}: graded interface thickness; n_G: number of layer comprising graded interface; X_i: distribution factor of graded interface.

Table 5
Nitrogen adsorption results of altered glass powder

Tests	Altered glass powder		Altered glass		Mean pore size (nm)
	S_{spe} ($m^2\ g_{AP}^{-1}$)	V_P ($cm^3\ g_{AP}^{-1}$)	S_{spe} ($m^2\ g_{AG}^{-1}$)	V_P ($cm^3\ g_{AG}^{-1}$)	
SON68-0.4 d	0.29 ± 0.01	0.00023 ± 0.00002	148 ± 1	0.15 ± 0.05	3.6
SON68-4 d	0.64 ± 0.05	0.00071 ± 0.00002	108 ± 1	0.11 ± 0.05	4.5
SON68-7 d	0.74 ± 0.02	0.00081 ± 0.00002	113 ± 1	0.11 ± 0.05	4.5
SON68-21 d	0.84 ± 0.01	0.00111 ± 0.00002	121 ± 1	0.16 ± 0.05	8.0
SON68-62 d	0.83 ± 0.03	0.00102 ± 0.00002	99 ± 1	0.13 ± 0.05	8.0

Results are reported to the total mass of altered glass powders (AP) and to the mass of altered glass (AG).

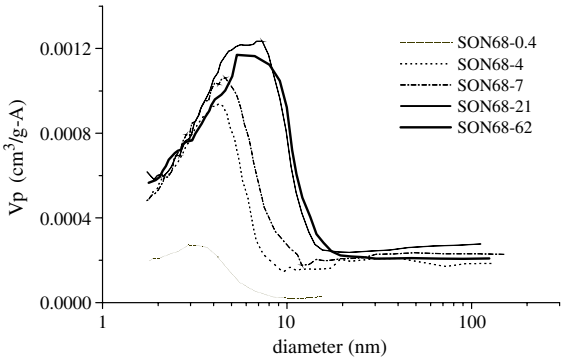

Fig. 6. Pores size distribution determined by BJH method for the dried altered glass powder, samples SON68-0.4 d to SON68-62 d.

3.3. Third step: gel densification

Altered glass thickness as a function of time presented in Fig. 3 shows a decreasing alteration rate between 4 and 7 days. The alteration rate drops by about two orders of magnitude ($r_{0(90\ °C,\ pH=9)}/360$) (Table 3). This decrease could be explained by an increase of the gel density. Sample SON68-7 w shows both an increase of the thickness and a densification of the alteration film (Table 4). This densification goes with a small increase of the graded interface thickness. The reflectivity curve of the dried sample SON68-7 d is very difficult to model. Drying can cause an increase of layer inhomogeneities, leading to adjustment parameter difficulties. Nevertheless, it can be concluded that there is a small contraction of the layer. This contraction cannot be quantified because of high experimental uncertainty (Table 4). The pore volume and specific surface area for the mass of altered glass powder increase (Table 5). Pore size distribution shows a mean pore diameter of 5 nm with a formation of larger pores as shown in Fig. 6.

The alteration film consists of de-alkalinized glass layer and a gel with a porosity similar to the gel of previous step, but presenting a higher density and a thicker graded interface (Fig. 7). The thickness increase of graded interface could explain the decreasing of alteration rate.

3.4. Fourth step: high alteration progress

At high alteration progress (21 and 62 days), the alteration rate becomes quasi-constant to reach the so-called residual rate [19]. For the SON68 glass, the alteration rate drops by more than three orders of magnitude (Fig. 3 and Table 3). Several hypotheses could explain the existence of this residual rate: the water diffusion in glass [20], the precipitation of secondary crystalline phases that consume elements from the protective gel layer and the evolution of the porous texture of the gel. In our samples, no secondary crystalline phases has been observed by SEM on the gel surface. The kinetics of formation of these phases can change from one experiment to another [21]. Here we retain the hypothesis of an evolution of the porosity.

3.4.1. Pore size increase

The reflectivity curve of sample SON68-21 w in situ at 21 days of alteration presents some low intensity fringes. The thickness e_R and density ρ_R of alteration film increase, and this is confirmed by results from solution analysis (Tables 3 and 4). The reflectivity curve of the same dried sample SON68-21 d exhibits a concave form (Fig. 4). This concave form can be attributed to the formation of a density gradient within the alteration layer. Porosity analysis of altered glass powder shows a smooth increase of pore volume and specific surface area per mass unit of altered glass powder. The pore size distribution shows the shift to larger pores with a mean diameter of 8 nm (Fig. 6). This observation can be related to the layer roughness (7 nm) obtained by simulation. This phenomenon cannot be assigned to an Oswald ripening process by dissolution–redeposition which should lead to an increase of the pore size associated with a decrease of the specific surface area and with a constant value of the pore volume. In our experiment, specific surface area and pore volume both increase. This phenomenon is assigned to the gel alteration.

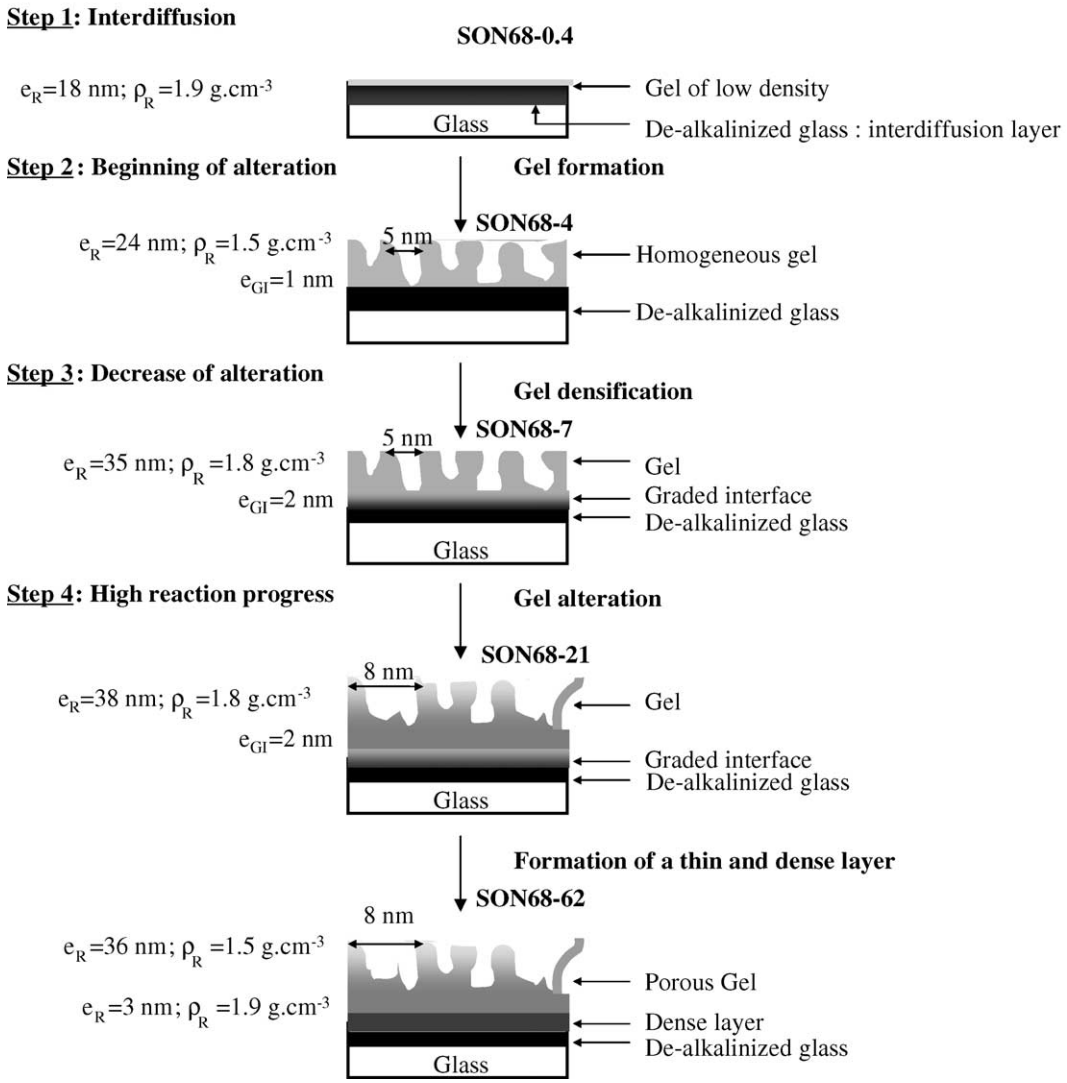

Fig. 7. Schematic representation of the different steps of the morphological evolution of SON68 glass altered layer, tests SON68-0.4 to SON68-62 w and d.

At this reaction progress, alteration film consists in de-alkalinized glass layer, a graded interface in a gel composed of an open porosity with a mean pore size of 8 nm diameter (Fig. 7).

3.4.2. Dense and thin layer formation within the gel

After 62 days of alteration the thickness of the altered glass increases smoothly. Intense concave forms on reflectivity curves of samples SON68-62 w and SON68-62 d can be related to the formation of a thin and dense layer (Figs. 4 and 5) [12,22,23]. Results from simulation for sample SON68-62 w show a 3 nm layer denser than the layer above (Table 4). An example of simulation without a 3 nm layer is shown in Fig. 8. Porosity results for the altered glass powder do not vary between 21 and 62 days. The dense layer might not be accessible to nitrogen, therefore the gel volume analyzed at 62 days could correspond to the less dense gel $\rho_R = 1.5\ g\,cm^{-3}$ also analyzed by nitrogen adsorption at 21 days.

At high reaction progress, the gel can be divided in two parts: a porous part with open porosity in contact with water and a denser part at the surface of de-alkalinized glass (Fig. 7).

3.5. Relation between a dense zone within the gel and a strong decrease in the alteration rate

The formation of a dense zone in gel which could constitute a diffusive barrier decreasing or blocking alteration is not specific to the SON68 glass alteration

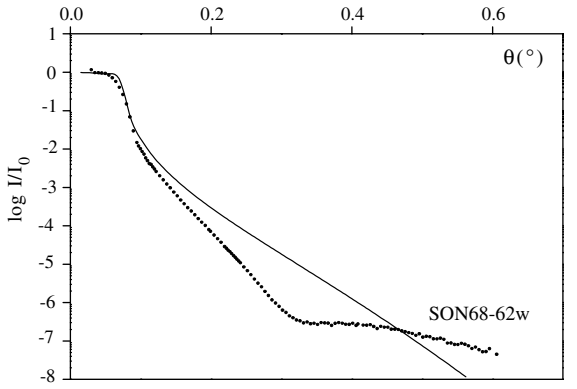

Fig. 8. Experimental and example of simulation with one layer for the sample SON68-62 w. $e_{R1} = 36$ nm and $\rho_{R1} = 1.5\ g\,cm^{-3}$, $\sigma_{air/1} = 7$ nm and $\sigma_{1/s} = 1.3$ nm (X wave line $\lambda = 0.06184$ nm).

film. Monte Carlo simulations, based on hydrolysis and recondensation probabilities of each element, of simple glasses, show an alteration blocking associated with a closing gel porosity (data not published). Reflectivity curves of altered glasses 1 and 2 are consistent with this phenomenon.

For glass 1 altered during 62 days, in the same conditions as those of SON68 glass, the concave form of the reflectivity curve and simulation results, are in agreement with a denser zone (Fig. 9). An example of simulated curve without a denser zone is also presented in Fig. 9 (glass 1 sim2). This zone is located between a thick gel in contact with water, and the glass. At this alteration progress, the rate has dropped by about three orders of magnitude compared with the initial dissolution rate (Table 3) [9].

For the glass 2 the alteration kinetics is different. After 15 days, the alteration completely stops (Fig. 1 and

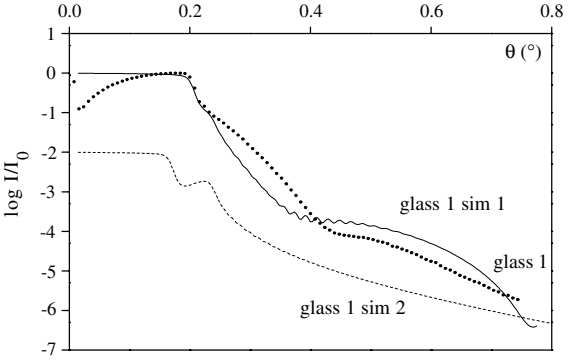

Fig. 9. Experimental (glass 1) and simulated reflectivity (glass 1 sim1 and glass 1 sim2 without a dense layer) curves of altered glass 1 (X wave line $\lambda = 0.15433$ nm).

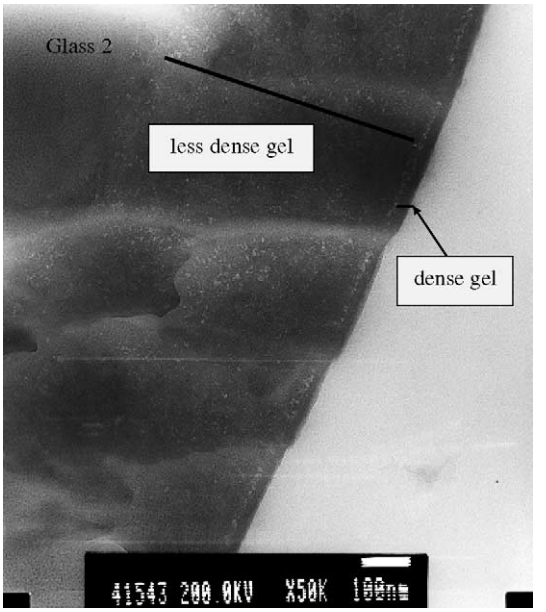

Fig. 10. TEM image of the altered layer of glass 2.

Table 3). Analysis of a glass sample altered during 62 days at 8000 m^{-1}, with transmission electronic microscopy, has shown two layers, one rather dense surface and another less dense layer underneath (Fig. 10). The layer located in surface is thick enough to be observed. The simulate reflectivity curve of glass 2 altered during 62 days (Fig. 11) is consistent with this dense layer and another layer less dense located below. Other simulations (glass 2 sim2 and sim3) with a single layer shows that the two-layers hypothesis is apparently more correct. The thin surface layer could constituted an

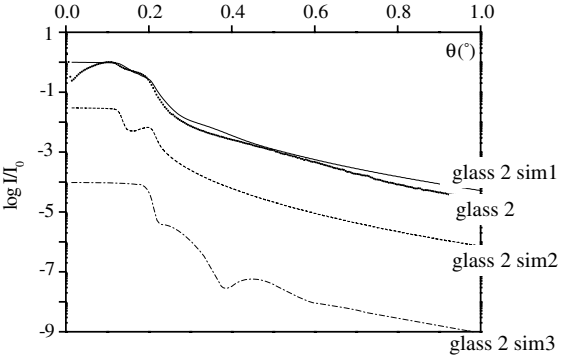

Fig. 11. Experimental (glass 2) and simulated (glass 2 sim1 and glass 2 sim2) reflectivity curves of altered glass 2. Glass 2 sim2: $e_{R1} = 370$ nm and $\rho_{R1} = 0.8\ g\,cm^{-3}$, $\sigma_{air/1} = 1$ nm and $\sigma_{1/s} = 0.5$ nm. Glass 2 sim3: $e_{R1} = 19$ nm and $\rho_{R1} = 1.3\ g\,cm^{-3}$, $\sigma_{air/1} = 3$ nm and $\sigma_{1/s} = 0.5$ nm (X wave line $\lambda = 0.15433$ nm).

alteration blocking zone. So far, explanation about this layer location is unknown.

Gel morphology seems to be strongly linked with the alteration kinetics and at glass composition which manage the competition between the diffusion of the species to the solution and their recondensation. The formation of a dense and thin zone, related with a decrease or a blocking in the alteration, brings some important information about the gel protective properties, even if the formation mechanisms are not clearly explained.

4. Conclusion

For the first time in situ XRR measurements were performed on alteration films. The coupling of XRR with nitrogen adsorption have brought some important and complementary information about the SON68 alteration film evolution. A morphological evolution of this alteration film and the formation of a thin and dense layer within the gel have been proposed from the XRR simulation results. This dense and thin layer could play the role of a diffusive barrier. In order to bring other evidence of this dense and thin layer for a very long alteration times, others analyses in situ by XRR will be carried out and coupled with grazing incidence small angle X-ray scattering to gain access to both open and closed porosities.

Acknowledgements

This study is cofunded by CEA and COGEMA companies. The authors are grateful to Ms La Bruquère from the University of Poitiers for TEM observations.

References

[1] F. Pacaud, N. Jacquet-Francillon, A. Terki, C. Fillet, Mater. Res. Soc. Symp. Proc. 127 (1989) 105.
[2] J.L. Nogues, PhD thesis, Université Montpellier II, 1984.
[3] L. Trotignon, PhD thesis, Université Paul Sabatier de Toulouse, 1990.
[4] S. Gin, PhD thesis, Université de Poitiers, 1994.
[5] E.Y. Vernaz, J.L. Dussossoy, Appl. Geochem. (Suppl. 1) (1992) 13.
[6] E.Y. Vernaz, N. Godon, Mater. Res. Soc. Symp. Proc. 257 (1992) 37.
[7] S.B. Xing, A.C. Buechele, I.L. Pegg, Mater. Res. Soc. Symp. Proc. 333 (1994) 541.
[8] S. Gin, Mater. Res. Soc. Symp. Proc. 663 (2001) 2207.
[9] S. Gin, C. Jegou, Water–Rock Interaction, Villasimius, Italy, 2001, p. 279.
[10] S. Gin, I. Ribet, M. Couillaud, J. Nucl. Mater. 298 (1&2) (2001) 1.
[11] S. Ribet, S. Gin, E. Vernaz, P. Chaix, R. Do Quang, GLOBAL 2001, 9–13 September 2001, Paris, France.
[12] D. Rebiscoul, A. Van Der Lee, P. Frugier, A. Ayral, S. Gin, J. Non-Cryst. Solids 325 (2003) 113.
[13] S. Lowell, J.E. Shields, Powder Surface Area and Porosity, Chapman & Hall, London, 1984.
[14] A. Van Der Lee, Solid-State Sci. 2 (2000) 257.
[15] IMD4.1 fit program: http://cletus.phys.columbia.edu~windt/idl.
[16] G. Ehret, J.L. Crovisier, J.P. Eberhart, J. Non-Cryst. Solids (1986) 72.
[17] T. Advocat, PhD thesis, Université Louis Pasteur de Strasbourg, 1991.
[18] E. Vernaz, J.L. Dussossoy, Appl. Geochem. Suppl. (1992) 13.
[19] S. Gin, P. Frugier, Mater. Res. Soc. Symp. Proc. 757 (2002) 8.
[20] B. Grambow, R. Muller, J. Nucl. Mater. 298 (2001) 112.
[21] O. Deruelle, O. Spalla, P. Barboux, J. Lambard, J. Non-Cryst. Solids 261 (2000) 237.
[22] D. Buttard, J. Eymery, F. Rieutord, F. Fournel, D. Lübbert, T. Baumbach, H. Moriceau, Physica B 283 (2000) 103.
[23] A. Van Der Lee, L. Hamon, Y. Holl, Y. Grohens, Langmuir (2001) 7664.